A complementary, two-method spherical approach to direction-based archeomagnetic dating

Yves Gallet, Maxime Le Goff

A complementary, two-method spherical approach to direction-based archeomagnetic dating

Yves Gallet, Maxime Le Goff

Université Paris Cité, Institut de Physique du Globe de Paris, CNRS, 1 rue Jussieu, F-75005 Paris, France

Abstract

We present a two-method spherical approach to archeomagnetic dating based on directional variations of the geomagnetic field after vector treatment of all data, including individual in situ structure-level data used to calculate the reference variation curve and the archeomagnetic direction to be dated. In this paper, the reference curve for France was determined from a compilation of data acquired from kiln structures using a sliding window technique in which the varying durations and time shifts between windows are fixed according to the temporal distribution of individual reference data, as well as the bivariate extension of Fisher's statistics. The first dating method involves identifying the time interval(s) in which the direction to be dated is closest to the mean directions that define the reference curve. The angles between the direction to be dated and reference curve directions, and the Fisher probability density function allow us to derive a coincidence probability density curve, from which it is possible to estimate a 95% probability level-based dating interval. The second dating method involves the determination of an archeomagnetic date in which the direction to be dated is statistically identical to a dated reference curve direction at the 95% confidence level. This approach is much more restrictive than the previous method because it requires an excellent agreement between the test and reference directions to obtain a dating result, while the first method is only based on relative proximity. Using examples of archeomagnetic

dating, we show that these two methods are complementarity and should be applied jointly to account for some of the limitations inherent in archeomagnetic dating, particularly due to the dispersion of the reference structure-level data.

Keywords

Archeomagnetic dating, geomagnetic directions, spherical statistics, maximum proximity, statistical compatibility

1. Introduction

Archeomagnetism allows for the recovery of information about ancient geomagnetic fields from the magnetic analysis of archeological artifacts that were fired during their manufacture or use (all types of kilns or artifacts such as pottery or architectural bricks). Archeomagnetism has two primary applications: in the context of geomagnetism, it can be used to characterize the temporal variations in the direction and/or intensity of the geomagnetic field through the analyses of dated artifacts; alternatively, in the context of archeology, our knowledge of the secular variation of the geomagnetic field can be used to propose an age for undated or poorly dated artifacts.

The first archeomagnetic studies with archeological applications were conducted by Giuseppe Folgheraiter, Paul-Louis Mercanton, Pierre David and Bernard Brunhes (Principe and Malfatti, 2020; Gallet, 2021); subsequently, the first attempts at archeomagnetic dating (i.e. the proposal of dates based on recent geomagnetic secular variation) date back to Raymond Chevallier's work on the chronology of volcanic flows on Mt. Etna (Chevallier, 1925; see also Gallet, 2021 for a discussion of early uses of archeomagnetism). The latter study was based on preliminary directional data, as well as the erroneous assumption that the geomagnetic field behaved periodically. The archeomagnetic dating of artifacts was further

explored in the 1960s, primarily in France and the United Kingdom under the leadership of Emile Thellier and Martin Aitken, respectively (e.g., Thellier, 1966; Aitken, 1970 and references therein). The development of archeomagnetic research in the past 25 years has been remarkable with the construction of increasingly detailed reference directional-variation curves of the geomagnetic field covering the past millennia for several regions of the world. The reference curves, however, are still mainly confined to Europe (e.g., Gallet et al., 2002; Hervé et al., 2013; Batt et al., 2017; Molina-Gardín et al., 2018; Le Goff et al., 2020; see also Brown et al., 2021). These curves offer increasingly interesting possibilities for archeomagnetic dating, a method that is now commonly, if not frequently, used by archeologists (e.g., Catanzariti et al., 2007 ; Gómez-Paccard et al., 2008; Tema et al., 2015; Aidona et al., 2018; Principe et al., 2018). They can also aid in determining the chronology and mapping of volcanic events (e.g. Tanguy et al., 2007; 2011). In addition, the construction of a detailed reference curve of geomagnetic intensity for Western Europe over the past two millennia has allowed archeomagnetic dating of ceramic objects displaced from their firing site, which otherwise prevents them from being dated archeomagnetically (Genevey et al., 2021). In the Near East, archeointensity studies conducted on much older pottery have also helped to constrain ceramic-based archeological chronologies (e.g. Shaar et al., 2020; Gallet et al., 2021).

This paper is limited to the discussion of direction-based archeomagnetic dating. We highlight some of the inherent limitations of archeomagnetic dating and propose the application of a dual spherical approach to improve the reliability of the dating results obtained.

2. Archeomagnetic direction measurements at the Institut de Physique du Globe de Paris

Over the past three years, directional archeomagnetic measurements have been carried out at the French National Magnetic Observatory, located in Chambon-la-Forêt and managed by the Institut de Physique du Globe de Paris (IPGP), using dedicated instruments that were developed and improved in the laboratory since its foundation at Saint Maur des Fossés by Emile Thellier (see Le Goff et al., 2020).

The experimental protocol used in the laboratory, initially established by Emile Thellier and later used by Ileana Bucur, is based on two principles. The first is that samples must be oriented as precisely as possible by determination of the horizontal plane and direction of geographic north to obtain accurate archeomagnetic directions. Hence, the samples have large sizes on the order of dm^3. They are systematically collected using a plaster cap technique (Thellier, 1967a; 1981). Dimensions of blocks collected in the field are adjusted in the laboratory to obtain standard samples 12 cm square with heights that integrate the entire thickness of the heated material within the studied structure, most often kilns. Structures built of bricks that were originally fired themselves are avoided in our laboratory. The magnetization of the samples is measured with an inductometer adapted to their large size (Thellier, 1967b; Le Goff, 1975). The orientation measurements made in the field are exactly preserved during preparation of the samples because no resampling is carried out, which is commonly done to make the sample size compatible with that required by conventional paleomagnetic instruments (~10 cm^3).

The second principle is based on the vast majority of the samples having only two types of magnetization: 1) a thermoremanent magnetization acquired during the last firing in the structure and 2) a viscous remanent magnetization linked to the spontaneous unblocking of the thermoremanent magnetization since the structure was last used, which is carried by a small fraction of magnetic grains. This viscous magnetization continuously follows the directional variations of the geomagnetic field, and increases in magnitude slowly with time

100 (e.g., Dunlop and Özdemir, 1997). It is therefore necessary to remove it to accurately measure
101 the thermoremanent magnetization, which is representative of the ancient geomagnetic field.
102 Rather than performing thermal or alternating field demagnetizations, as is usually the case in
103 paleomagnetism, we perform magnetic viscosity experiments within a laboratory field, which
104 are particularly effective in reliably isolating the thermoremanent magnetization (see
105 discussion and details in Le Goff et al., 2020). We must emphasize that the aim of our paper
106 is not to elaborate upon the advantages or disadvantages of the experimental method, from
107 which almost all the data used below were derived, but rather to more generally present the
108 utility of the dual approach that we are proposing for archeomagnetic dating.

109 Following the work of Thellier (1981) and Bucur (1994), we have studied approximately
110 500 kilns found in mainland France over the past 25 years. These kilns are comprised mainly
111 of domestic and pottery kilns whose ages extends back over the past two millennia (see
112 details in Le Goff et al., 2020). To calculate a reference directional-variation curve of the
113 geomagnetic field for France, we applied the conclusions of Le Goff and Gallet (2019) to its
114 temporal resolution, and retained only results dated to less than ± 50 years by archeologists.
115 The resulting "Saint Maur" data compilation comprises almost 300 archeomagnetic
116 directions. After applying a Virtual Geomagnetic Pole reduction of all data to a single
117 reference site (Paris), the reference curve was calculated using a sliding window method, with
118 window durations and time shifts adjusted according to the temporal distribution of the data
119 (Le Goff et al., 2002; 2020). For each time window, an average archeomagnetic direction
120 (described by its inclination, I, and its declination, D) and its 95%-confidence ellipse were
121 calculated by weighting the individual data (i.e., measurements obtained at the structure level)
122 based on the proportion of time an individual datum is contained in a window and using the
123 bivariate extension of Fisher's statistics (Le Goff, 1990; Le Goff et al., 1992). The usual
124 elongated shape of each ellipse allows one to account for possible drift of the geomagnetic

directions during the duration of each window. The succession of ovals obtained, encompassing the period ranging from the first century BCE to 1700 AD, forms the French reference curve (Fig. 1), and its linear interpolation every 10 years is now commonly used for archeomagnetic dating. It is worth mentioning that the dispersion of the confidence circles of the individual structure-level directions used to calculate the curve is confined to a maximum envelope of about 3° around the mean curve (see Fig. 7 and discussion in Le Goff et al., 2020). Any archeomagnetic direction to be dated should be located within this envelope.

3. A dual spherical approach to archeomagnetic dating

In general, any directional-based archeomagnetic dating relies on the comparison between the archeomagnetic direction (I, D, α_{95}) obtained for a fired structure of unknown age and the reference directional variation curve determined for the geographic area or country in which the structure originated. In some cases, the reference curve used is derived from either a regional or global geomagnetic field model (e.g., Pavón-Carrasco et al., 2009). It should be noted that a Bayesian method of dating based on the calculation of an *a posteriori* age distribution has also been developed (Lanos, 2004; Lanos et al., 2005; Schnepp et al., 2015; Hervé and Lanos, 2017; Livermore et al., 2018). This technique, known as marginalization dating, has recently been applied to archeointensity data (e.g., Gallet et al., 2020; 2021; Shaar et al., 2020; Genevey et al., 2021).

In commonly used archeomagnetic dating methods, the reference curve, no matter how it is calculated, is separated into two curves, one for declination and another for inclination, each with their respective error bars (e.g., Pavón-Carrasco et al., 2011 and references above). Archeomagnetic dates are then deduced from the product of the probability density distributions determined separately for the declinations and inclinations of the structures

149 being dated. In some cases, this methodology also includes the probability density distribution
150 obtained for archeointensities.

151 Here, however, we have chosen to use spherical statistics by comparing directional data
152 without dissociating inclinations from declinations (Le Goff et al., 2002). Two dating
153 methods are compatible with the oval time-window technique used to calculate the French
154 reference directional-variation curve. In both cases, the values of the precision parameter K
155 for the reference directions determined using the bivariate extension of Fisher's statistics must
156 be adjusted. To do this, from the direction of the elongation of each 95% confidence oval and
157 the associated maximum and minimum values of K, we consider the value of K (referred to as
158 K_{ref} below) in the direction of the great circle passing through the reference direction and the
159 direction to be dated (see equation 5 in Le Goff et al., 2002). The general principles of the
160 first method, which provides a maximum proximity-based dating estimate, are similar to the
161 technique described above: it identifies the time period(s) in which the direction being dated
162 is closest to the mean directions that define the reference curve, taking into account their 95%
163 margins of error. We use a simple statistic derived from the distribution of directions
164 according to the Fisher probability density function (see for instance equation 6.5 in Butler,
165 1992). For each pair formed by a reference direction (with its precision parameter K_{ref}) and
166 the direction to be dated (with its precision parameter referred to as K_{dat}), we calculate a
167 probability of coincidence as the product of $\exp[K_{ref}(\cos\gamma - 1)]$ with $\exp[K_{dat}(\cos\gamma - 1)]$, γ
168 being the angle between the two directions. The successive reference directions then allow us
169 to obtain a coincidence probability density curve, from which it is possible to establish a 95%
170 probability-level dating interval on the basis of a surface calculation. As each oval of the
171 directional variation curve is associated with a time window in addition to a central date, this
172 interval is extended at its ends by half the window durations concerned. Note that the 95%
173 confidence level depends on the nature of the variations over the time interval tested. The

174 latter can be adjusted (i.e., reduced) depending on independent chronological constraints (e.g.,
175 archeological constraints, radiocarbon and/or thermoluminescence dating).

176 The second approach that we developed (Le Goff et al., 2002) involves determining an
177 archeomagnetic dating estimate when the direction being dated is statistically identical to a
178 dated direction of the reference curve at the 95% confidence level; specifically, when the
179 angle between them is less than a certain critical value (γ_c) based on the statistical
180 characteristics of the directions considered (McFadden and McElhinny, 1990; see equations 1
181 and 2 and detailed description in Le Goff et al., 2002). The dating interval obtained is
182 extended by half the window duration of the mean reference direction at each end. This
183 approach is much more restrictive than the first method because it requires excellent
184 agreement between the test and reference directions, whereas the first method is based only
185 on relative proximity. In addition, contrary to the first method, any dated time interval
186 determined by statistical compatibility, or equivalence, at the 95% confidence level is
187 completely independent of the other time segments of the reference curve. This calculation is
188 a statistical test that validates, with a fixed level of confidence, the hypothesis that the dating
189 range obtained cannot be rejected (McFadden and McElhinny, 1990; Le Goff et al., 2002).
190 Hence, it also provides information on a more likely age range(s) within the 95%-confidence
191 time segment (referred to as $\gamma<\gamma_c$ Probability in the figures below), which is information that
192 can be prudently conveyed to the archeologists (Le Goff et al., 2002). Examples of these two
193 archeomagnetic dating methods are illustrated below.

194

195 **4. Discussion based on examples of archeomagnetic dating**

196 The first example of archeomagnetic dating involves a large domestic oven more than two
197 meters wide that was excavated from natural silt near the small town of Anet, ~70 km west of

198 Paris, France (Labat, 2021). This oven had four superimposed floors separated by pebble
199 beds, three of which were sampled for archeomagnetic analysis (Table S1). The results
200 obtained for the upper floor (the last use of the oven, before its abandonment) are presented in
201 Fig. 2a. The two dating approaches yield similar results, suggesting a date between the mid-
202 10th and mid-12th centuries, with a higher probability for the 11th century. These
203 archeomagnetic dating results are consistent with the few elements of archeological dating
204 from pottery fragments found in the kiln (Labat, 2021).

205 However, there are some cases in which it may not be possible to obtain dates from both
206 dating methods. To illustrate this synthetically, we have arbitrarily modified the magnetic
207 declination of the direction used in Fig. 2a by 2° (Fig. 2b) and 4° (Fig. 2c) towards the east,
208 resulting in the gradual deviation of the undated direction from the reference curve. At a
209 deviation of 2°, it is no longer possible to determine a date by statistical compatibility because
210 the undated direction is no longer 95% compatible with a dated segment of the reference
211 curve. Maximum proximity dating can still be used, giving a result that is very close to the
212 previously derived dating estimate while remaining just as precise, even if the direction is
213 quite far from the reference curve (Fig. 2c). An actual example is also presented in Fig. 3
214 involving the archeomagnetic dating of a domestic oven found at Genas, near Lyon, in
215 central-eastern France (Donzé, 2021; Table S1). It is extremely important to emphasize that
216 dating by maximum proximity always produces a result unless a rejection distance is
217 introduced. When observed, the interpretation of the apparent divergence between the
218 direction being dated and the reference curve is far from trivial. Causes of such a discrepancy
219 should be sought, both in terms of the direction to be dated and/or the reference curve. For
220 example, the sampled structure may have been slightly tilted since its last use, thus causing a
221 deviation of the archeomagnetic direction. Alternatively, this direction could be slightly
222 biased, perhaps due to an anisotropy effect during the acquisition of thermoremanent

magnetization, which would remain present and would not be sufficiently corrected. In terms of the reference curve, it may be the case that the curve is insufficiently well defined at the corresponding age, or its estimated accuracy does not satisfactorily reflect the current state of our knowledge. Indeed, some of the directions used to calculate the reference curve may themselves be slightly biased by one of the reasons mentioned above. In addition, one can also consider the distribution of the individual structure-level data used to construct the reference curve (Fig. 7 in Le Goff et al., 2020), especially in terms of the significance of the apparent discrepancy observed. It could result from the smoothing procedure (i.e., the sliding windows technique) used to construct the reference curve, which constrains its temporal resolution (Le Goff and Gallet, 2019). In other words, the absence of statistical compatibility dating does not necessarily mean that the direction to be dated does not fall within the usual dispersion envelope of the data used to calculate the curve. From this perspective, the undated directions used in Figs. 2b, 2c and 3 do not appear to be particularly deviant from the set of individual reference directions available for the periods studied (Fig. 4). This shows us that, in addition to their number and consistency, the effects of the temporal distribution of the reference data on the calculation of the mean directional curve using a sliding window technique should not be ignored. In fact, dispersion of the reference data is clearly a key consideration (see appendix). Regardless, the lack of results from 95% confidence level statistical compatibility dating is an important aspect that should be recognized when discussing the reliability of dating results. However, although it would seem preferable to focus primarily on results of the statistical compatibility dating, results obtained by the maximum proximity method are at least equally interesting and significant because this technique, to some extent, minimizes some of the inherent limitations of archeomagnetic dating due to the dispersion of reference data. Above all, this demonstrates that the two methods are complementary and should be applied in conjunction.

When applicable, both dating methods should give similar results. However, depending on the nature of the reference curve, there are cases in which statistical compatibility dating gives more accurate results. These cases involve periods in which the directional variation curve is described by a hook or a cusp, as during the Roman period or during the 13th-14th centuries (Fig. 1). Fig. 5a illustrates archeomagnetic dating of a Roman kiln discovered at Plessis-Gassot, ~20 km north of Paris (Gazagne, 2021; Table S1). Maximum proximity dating suggests a long-term interval between ~50-465 AD, while statistical compatibility dating gives two distinct intervals, ~70-260 AD and ~295-465 AD. The maximum proximity probability curve shows two clear peaks that fall within the Early and Late Roman Empire periods (dark red curve), which is synchronous with the two previous options. The 95% probability threshold, however, approximately incorporates both of these solutions within the same 95% dating interval. This is an inevitable consequence of the dependence of the 95% probability level calculated for maximum proximity dating on the nature of the directional variations during the entire time segment tested for dating (in this case, between 120 BCE and 800 AD). Two synthetic examples for the Roman (Fig. 5b; Table S1) and Medieval (Fig. 5c; Table S1) periods more clearly illustrate this situation, further emphasizing how these two methods complement each other.

Each example presented in Figs. 2, 3 and 5 provides specific chronological information. Series of archeomagnetic dating results are also of interest because of the increasing wealth of information thus obtained for the purpose of archeological consideration. As mentioned above, the oven discovered at Anet exhibited well-separated, successive levels of use. This raises the question of whether the duration this oven was used can also be constrained by archeomagnetism, and how the maximum proximity and statistical compatibility dating methods help respectively to limit this duration. The dating results from three of the four floors, including the upper (see also Fig. 2a) and lower floors, are presented in Fig. 6. Both

dating methods produce results for each of the three levels. All dating estimates obtained are very consistent and there is no apparent drift in the archeomagnetic directions suggesting a change in the 95% dating intervals that could be related to a long period of oven use. With the precision of archeomagnetism, as well as considering the nature of the reference directional variations over the time period studied, the three levels are found to have roughly the same age, implying that the oven was not used for a long time. However, this duration cannot be estimated precisely from archeomagnetic data alone. A *terminus post quem* is defined at ~1000 AD (oldest limit of the time interval derived from statistical compatibility dating of the lower floor) and a *terminus ante quem* at ~1125 AD (youngest dating limit of the upper floor), giving a maximum duration of ~125 years, while maximum proximity dating suggests a maximum period of use of ~195 years (i.e., ~945-1140 AD). It is important to remember that these estimates must also be added to the duration of use of the first state/level of the kiln, which is currently unknown. While it seems more likely that this kiln was not used for such a long duration, the accuracy of these archeomagnetic constraints is clearly penalized by the temporal resolution of the reference directional variation curve (Le Goff and Gallet, 2019 and see above).

The large-scale use of archeomagnetic dating for numerous domestic ovens from the same archeological site can also provide constraints on the continuity or possible discontinuities in site occupation. Examples based on studies conducted by Nicolas Warmé (Institut National de Recherches Archéologiques Préventives, INRAP) can be found in Le Goff et al. (2020) and are not shown here.

5. Concluding remarks

296 The examples presented above highlight the applications of archeomagnetic dating in
297 terms of the vector treatment of directions, specifically when the compared directions (the
298 direction to be dated and a mean reference direction) are made to be as equivalent as possible.
299 This can be accomplished by using the sliding window and averaging technique developed by
300 Le Goff et al. (2002; 2020), which involves the weighting of individual (structure-level)
301 reference data within the same time window. In addition to providing a direct description of
302 the consistency between two directions, this procedure allows for the application to
303 archeomagnetic dating of the statistical compatibility test developed by McFadden and
304 McElhinny (1990), which compares two paleomagnetic directions (Le Goff et al., 2002). This
305 contrasts with the usual procedure of comparing declinations and inclinations separately,
306 although this difference in data processing does not significantly alter the dating results
307 derived from the maximum proximity method (tests were performed using the code
308 developed by Pavón-Carrasco et al., 2011). It should be noted that both of our proposed
309 spherical methods require a complete determination of the archeomagnetic direction to be
310 dated, whereas the dating methods developed by Pavón-Carrasco et al. (2011) and Lanos and
311 Dufresne (2019) can be applied with a single directional element, declination or inclination,
312 and possibly with intensity data (e.g. Tema et al., 2013).

313 Based on this spherical approach, we show the importance of the combined application of
314 two dating methods: maximum proximity dating, which is similar (although with differences)
315 to the usual archeomagnetic dating procedure, and statistical compatibility dating, which is
316 derived from the test developed by McFadden and McElhinny (1990). While they normally
317 should give similar results, the more restrictive statistical compatibility method may not
318 always produce results due to the 95% confidence level requirement, whereas the maximum
319 proximity method always gives results, even if the undated direction deviates significantly
320 from the reference curve. A clear advantage of the latter is that it may partially circumvent

limitations related to the dispersion of the reference data and to its smoothing by successive time windows. Thus, both methods have their advantages and disadvantages, and ideally should be jointly applied to provide a powerful alternative to other archeomagnetic dating methods. While the absence of statistical compatibility dating may be taken as a warning regarding the reliability of an archeomagnetic dating result, we prefer to adopt a more positive point of view in which statistical compatibility dating, when available, allows us to define an optimal time range within the tested interval.

Archeomagnetic dating remains a difficult exercise, and any results must be interpreted cautiously. Archeomagnetists cannot control crucial elements such as a slight tilting of a structure (which may be visually undetectable) since its last use, which introduces biases into archeomagnetic dating results, or the temporal resolution of the reference directional variation curve. Le Goff and Gallet (2019) used a synthetic approach to show that the overall dating accuracy of the reference data would not allow for the recovery of rapid, century-scale directional variations that would be consistent with the well-known evolution of the geomagnetic field over the past few centuries (even when using age uncertainties of only ±50 years and despite numerous reference data). These elements, as well as the concerns regarding the dispersion of reference data, mean that archeomagnetic dating results must necessarily be compared with those obtain by other chronological methods (e.g., archeological, historical, radiocarbon and/or thermoluminescence).

Recent progress in establishing regional directional variation curves of the geomagnetic field for the past few millennia has allowed the improvement of archeomagnetic dating methods as well as their integration into the list of chronological methods available to archeologists. The proposed dual spherical dating approach used in this study allows us to enhance the reliability of the results obtained and thus strengthen the scope of archeomagnetic dating.

Acknowledgements

We are grateful to Agnès Genevey (LAMS, CNRS) for helpful and stimulating discussions as well as to Nicolas Warmé (INRAP) for our long journey in archeomagnetism. We thank Olivier Labat (Institut National du Patrimoine), Pierre-Alain Donzé (Eveha, Etudes et Valorisations Archéologiques) and Damien Gazagne (Eveha) for allowing us to collect archeomagnetic samples. We also thank Jonathan Hagstrum and an anonymous reviewer for helpful comments on the manuscript.

References

Aidona, E., Polymeris, G., Camps, P., Kondopoulou, D., Ioannidis, N., Raptis, K., 2018. Archaeomagnetic versus luminescence methods: the case of an Early Byzantine ceramic workshop in Thessaloniki. Greece. Archaeological and Anthropol. Sci. 10.

Aitken, M., 1970. Dating by archaeomagnetism and thermoluminecent methods. Phil. Trans. Roy. Soc. Lond. A 269, 77-88.

Batt, C.M., Brown, M.C., Clelland, S.-J., Korte, M., Linford, P., Outram, Z., 2017. Advances in archaeomagnetic dating in Britain: New data, new approaches and a new calibration curve. J. Archaeolog. Sci. 85, 66–82.

Brown, M., Hervé, G., Korte, M., Genevey, A., 2021. Global archaeomagnetic data: the state-of-the-art and future challenges. Phys. Earth Planet. Inter., 318, 106766.

Bucur, I., 1994. The direction of the terrestrial magnetic field in France during the last 21 centuries. Phys. Earth Planet. Inter. 87, 95-109.

368 Catanzariti, G., McIntosh, G., Osete, M., Nakamura, T., Rakowski, A., Gonzalez, I., Lanos,
369 P., 2007. A comparison of radiocarbon and Archaeomagnetic dating from an
370 archaeological site in Spain. Radiocarbon 49 (2), 543–550.

371 Chevallier, R., 1925. L'aimantation des laves de l'Etna en Sicile du XIIe au XVIIe siècles.
372 Ann. Phys. Fr. Xe série IV, 162 pp.

373 Donzé, P.-A., 2021. Genas (Rhône). 1, rue de la République , Archéologie médiévale 51 ,
374 185-186.

375 Dunlop, D, Özdemir, O, 1997. Rock magnetism, Fundamental and Frontiers. Cambridge
376 Univ. Press, 573 pp.

377 Gallet, Y., Genevey, A., Le Goff, M., 2002. Three millennia of directional variation of the
378 Earth's magnetic field in western Europe as revealed by archeological artifacts. Phys.
379 Earth. Planet. Inter. 131, 81-89.

380 Gallet, Y., Fortin, M., Fournier, A., Le Goff, M., Livermore, P., 2020. Analysis of
381 geomagnetic field intensity variations in Mesopotamia during the third millennium BC
382 with archeological implications. Earth Planet. Sci. Lett. 537, 116183.

383 Gallet, Y., Fournier, A., Livermore, P.W., 2021. Tracing the geomagnetic field intensity
384 variations in Upper Mesopotamia during the Pottery Neolithic to improve ceramic-based
385 chronologies. J. Archaeol. Sci. 132, 105430.

386 Gallet, Y., 2021. The dawn of archeomagnetic dating. C. R. Geoscience 353 (1), 285-296.

387 Gazagne, D., 2021. Le Plessis-Gassot – Site REP/SNC, route d'Écouen. ADLFI, Archéologie
388 de la France, http://journals.openedition.org/adlfi/112437.

389 Genevey, A., Gallet, Y., Thébault, E., Livermore P.W., Fournier, A., Jesset, S., Lefèvre, A.,
390 Mahé-Hourlier, N., Marot, E., Regnard S., 2021. Archeomagnetic intensity investigations

391 of French Medieval ceramic workshops: Contribution to regional field modeling and
392 archeointensity-based dating. Phys. Earth Planet. Inter. 318, 106750.

393 Gómez-Paccard, M., Beamud, E., 2008. Recent achievements in archaeomagnetic dating in
394 the Iberian Peninsula: application to Roman and Mediaeval Spanish structures. J.
395 Archaeol. Sci. 35, 1389-1398.

396 Hervé, G., Chauvin, A., Lanos, P., 2013. Geomagnetic field variations in Western Europe
397 from 1500 BC to 200 AD. Part I: directional secular variation curve. Phys. Earth Planet.
398 Inter. 218, 1–13.

399 Hervé, G., Lanos, P., 2017. Improvements in Archaeomagnetic Dating in Western Europe
400 from the Late Bronze to the Late Iron Ages: An Alternative to the Problem of the
401 Hallstattian Radiocarbon Plateau. Archaeometry 60 (4), 870-883.

402 Labat, O., 2021. Anet Sente des Duvaux. ADLFI. Archéologie de la France,
403 http://journals.openedition.org/adlfi/44508.

404 Lanos, P., 2004. Bayesian inference of calibration curves: application to archaeomagnetism.
405 In Tools for constructing chronologies: crossing disciplinary boundaries, C. Buck and A.
406 Millard Eds. Springer-Verlag, London vol. 17, 43–82.

407 Lanos, P., Le Goff, M., Kovacheva, M., Schnepp, E., 2005 Hierarchical modelling of
408 archaeomagnetic data and curve estimation by moving average technique. Geophys. J.
409 Int. 160, 440–476.

410 Lanos, P., Dufresne, P., 2019. ChronoModel version 2.0 User manual. pp. 84, HAL id: hal-
411 02058018.

412 Le Goff, M., 1975. Inductomètre à rotation rapide continue pour la mesure des faibles
413 aimantations rémanentes et induites en magnétisme des roches. Mém. Diplôme
414 d'Ingénieur CNAM Paris, 85 pp.

Le Goff, M., 1990. Lissage et limites d'incertitude des courbes de migration polaire: pondération des données et extension bivariante de la statistique de Fisher. C. R. Acad. Sci. Sér. II 311, 1191-1198.

Le Goff, M., Henry, B., Daly, L., 1992. Practical method for drawing a VGP path. Phys. Earth Planet. Int. 70, 201–204.

Le Goff, M., Gallet, Y., Genevey, A., Warmé, N., 2002. On archaeomagnetic secular variation curves and archaeomagnetic dating. Phys. Earth Planet. Inter. 134, 203-211.

Le Goff, M., Gallet, Y., 2017. A reappraisal of instrumental magnetic measurements made in Western Europe before AD 1750: confronting historical geomagnetism and archaeomagnetism. Earth Planets and Space 69, 32

Le Goff, M., Gallet, Y., 2019. On the resolution of regional archaeomagnetism: untangling directional geomagnetic oscillations and data uncertainties using the French archaeomagnetic database for dates between AD 1000 and 1500 as a guide. Geological Society, London, Special Publications, 497.

Le Goff, M., Gallet, Y., Warmé, N., Genevey, A., 2020. An updated archeomagnetic directional variation curve for France over the past two millennia, following 25 years of additional data acquisition. Phys. Earth Planet. Inter. 309, 106592.

Livermore, P.W., Fournier, A., Gallet, Y., Bodin, T., 2018. Transdimensional inference of archeomagnetic intensity change. Geophys. J. Int. 215, 2008-2034.

McFadden, P., McElhinny, M., 1990. Classification of the reversal test in palaeomagnetism. Geophys. J. Int. 103, 725–729

Molina-Cardín, A., Campuzano, S. A., Osete, M. L., Rivero-Montero, M., Pavón-Carrasco, F. J., Palencia-Ortas, A., Martín-Hernández, F., Gómez-Paccard, M., Chauvin, A., Guerrero-Suárez, S., Pérez-Fuentes, J. C., McIntosh, G., Catanzariti, G., Sastre Blanco, J. C.,

439 Larrazabal, J., Fernández Martínez, V. M., Álvarez Sanchís, J. R., Rodríguez-Hernández,
440 J., Martín Viso, I., Garcia i Rubert, D., 2018. Updated Iberian Archeomagnetic
441 Catalogue: New Full Vector Paleosecular Variation Curve for the Last Three Millennia.
442 Geochem. Geophys. Geosyst. 19, 10, 3637-3656.

443 Pavón-Carrasco, F. J., Osete, M. L., Torta, J. M., Gaya-Pique, L.R., 2009. A regional
444 archeomagnetic model for Europe for the last 3000 years, SCHA.DIF.3K: Applications to
445 archeomagnetic dating. Geochem. Geophys. Geosyst. 10, Q03013.

446 Pavón-Carrasco, F. J., Rodríguez-González, J., Osete, M. L., Torta, J. M., 2011. A matlab tool
447 for archeomagnetic dating. J. Archeol. Sci. 38 (2), 408–419.

448 Principe, C., Gogichaishvili, A., Arrighi, S., Devidze, M., La Felice, S., Paolillo, A.,
449 Giordano, D., Morales, J., 2018. Archaeomagnetic dating of copper age furnaces at Croce
450 di papa village and relations on Vesuvius and Phlegraean fields volcanic activity. J.
451 Volcanol. Geotherm. Res. 349, 217–229.

452 Principe, C., Malfatti, J., 2020. Guiseppe Folgheraiter: The Italian pioneer of
453 archaeomagnetism. Earth Sci. History 39 (2), 1-30.

454 Schnepp, E., Obenaus, M., Lanos, P., 2015. Posterior archaeomagnetic dating: An example
455 from the Early Medieval site Thunau am Kamp, Austria. Journal of Archaeological
456 Science: Reports 2, 688-698.

457 Shaar, R., Bechar, S., Finkelstein, I., Gallet, Y., Martin, M. A. S., Ebert, Y., Keinan, J.,
458 Gonen, L., 2020. Synchronizing geomagnetic field intensity records in the Levant
459 between the 23rd and 15th centuries BCE: chronological and methodological implications.
460 Geochem. Geophys. Geosyst. 21, e2020GC009251.

461 Tanguy, J.-C., Condomines, M., Le Goff, M., Chillemi, V., Le Delfa, S., 2007. Mount Etna
462 eruptions of the last 2,750 years: revised chronology and location through archeomagnetic

and ^{226}Ra-^{230}Th dating. Bull. Volcanol. 70, 55-83.

Tanguy, J.-C., Bachèlery, P., Le Goff, M., 2011. Archeomagnetism of piton de la Fournaise: bearing on volcanic activity at La Réunion Island and geomagnetic secular variation in southern Indian Ocean. Earth Planet. Sci. Lett. 303, 361–368.

Tema, E., Fantino, F., Ferrara, E., Lo Giudice, A., Morales, J., Goguitchaichvili, A., Camps, P., Barello, F., Gulmini, M., 2013. Combined archaeomagnetic and thermoluminscence study of a brick kiln excavated at Fontanetto Po (Vercelli, Northern Italy). J. Archael. Sci. 40, 2025-2035.

Tema, E., Polymeris, G., Morales, J., Goguitchaichvili, A., Tsaknaki, V., 2015. Dating of ancient kilns: a combined archaeomagnetic and thermoluminescence analysis applied to a brick workshop at Kato Achaia, Greece. J. Cult. Herit. 16 (4), 496–507.

Thellier, E., 1966. Le champ magnétique terrestre fossile. Nucleus 7, 1-35.

Thellier, E., 1967a. Methods of sample collection and orientation for Archaeomagnetism. Methods in Palaeomagnetism, Elsevier Amsterdam, 16-21.

Thellier, E., 1967b. A big sample spinner magnetometer. In Methods in Palaeomagnetism, Elsevier Amsterdam, 149-154.

Thellier, E., 1981. Sur la direction du champ magnétique terrestre en France durant les deux derniers millénaires. Phys. Earth Planet. Inter. 24, 89-132.

Appendix : Further illustrating reference data dispersion

We have highlighted the effects of reference data dispersion on archeomagnetic dating results, particularly in the case of the two spherical methods proposed. Here, we illustrate this dispersion in more detail by using the Bayesian AH-RJMCMC (Age Hyperparameter Reverse Jump Monte Carlo Markov Chain) method developed by Livermore et al. (2018) to trace the regional change in geomagnetic intensities over the past millennia (e.g. Gallet et al., 2020; Genevey et al., 2021). This method relies on fitting reference data without *a priori* information (and without regularization) about the curve to be determined (see detailed description of the method in Livermore et al., 2018). In applying it to geomagnetic directions, declination and inclination data were separated.

The resulting time-dependent posterior distributions of declination and inclination are shown in Fig. A (the calculation parameters are given in its legend). They appear to be bimodal and/or particularly spread out at certain periods. This can be clearly seen around 450, 1000-1200, and 1500 AD for the inclinations, and around the 12th century for the declinations (see discussion in Le Goff and Gallet, 2019). These features thus directly represent the dispersion of data. Unless erratic evolutions of the geomagnetic declinations and inclinations on a short time scale are considered, it is necessary to smooth the dataset. Thus, the sliding window method in which the duration and time shifts between the windows are varying according to the temporal distribution of the reference data provides a conservative, and reasonable, approach to recovering the regional geomagnetic field curve in a form that is suitable for archeomagnetic dating.

Figure captions

Fig. 1. Directional variations of the Earth's magnetic field in France between 100 BCE and 1700 AD as derived from the archeomagnetic data compiled by Le Goff et al. (2020). The mean curve was calculated from the bivariate extension of Fisher statistics (see Le Goff et al., 2002 and 2020 for details). The 95%-confidence ovals are reported based on the weighted number of structure-level data available per time window. Between 1700 and 2000 AD, geomagnetic directions are known from direct (instrument) data (light green curve; Le Goff and Gallet, 2017). All data were reduced to Paris.

Fig. 2. (a) Archeomagnetic dating of the upper floor of the domestic oven found at Anet, France (Labat, 2021; Table S1). Synthetic examples of dating after arbitrary (b) 2° shift and (c) 4° shift in the declination toward the east are also presented. The direction to be dated (α_{95} in thick black line) and the set of mean directions that define the geomagnetic reference directional variation curve in France (Le Goff et al., 2020) are shown in a spherical projection. The segment tested for maximum proximity dating (here between 700 and 1500 AD) is shown in red, the corresponding 95%-confidence ovals are shown in light blue, and the rest of the curve, without the confidence ovals, is shown in gray. The diagrams on the right show the dating results. In each of these diagrams, the thin dark red curve indicates the normalized maximum proximity probability density curve (x100) determined between the direction to be dated and all reference directions. The thick horizontal dark red line indicates the maximum proximity dating interval determined to the 95% probability level. The blue curve shows the angular distances between the direction to be dated and all reference directions minus the associated critical distances that are determined with 95% confidence

(McFadden and McElhinny, 1990). Dating is only possible when these values are negative (Le Goff et al., 2002). The thick horizontal blue line indicates the extension of the dating interval obtained by 95%-statistical compatibility. The green curve shows what is called here $\gamma < \gamma_c$ Probability, i.e. the errors (%) that would be made if the direction to be dated was considered to be different from the successive reference directions (Le Goff et al., 2002).

Fig. 3. Archeomagnetic dating of a domestic oven found in Genas, Central France (Donzé, 2021; Table S1). The segment tested for maximum proximity dating is between 600 and 1400 AD. This figure uses the legend described in Fig. 2.

Fig. 4. Dispersion of the available individual (structure-level) data between 600 and 1400 AD used to calculate the mean sliding window directional variation curve (same as in Fig. 1). These data are color-coded according to their dating ranges. The data in white and gray are from Anet and Genas, respectively, and are also shown in Figs. 2 and 3.

Fig. 5. (a) Archeomagnetic dating of a Roman oven found at Plessis-Gassot (Gazagne, 2021). The segment tested for maximum proximity dating is between 120 BCE and 800 AD, and uses the same legend as described in Fig. 2. The synthetic dating of two arbitrary archeomagnetic directions is also presented, which would indicate (b) a Roman age and (c) a Medieval age (Table S1). In Fig. 5c, only one maximum-proximity dating interval is retained due to an overlap between the two intervals derived from surface computations when extended by half the window durations at their ends. The same situation actually occurs in Fig 5a,b as well, but very marginally so.

Fig. 6. Archeomagnetic dating of three of the four floors of the domestic oven found at Anet (Labat, 2021; Table S1). (a) Dating of the upper floor (see also Fig. 2a); (b) dating of one of the two intermediate floors; (c) dating of the lower floor. This figure uses the legend described in Fig. 2.

552 **Fig. A.** Density of posterior distributions of declination and inclination between 120 BCE and
553 1700 AD as estimated using the Bayesian AH-RJMCMC method developed by Livermore et
554 al. (2018) and the compiled Saint Maur data with age uncertainties of less than ±50 years. The
555 densities are reported in greyscale, with darker shades for higher values. The blue dashed
556 lines indicate the 95%-credible envelope. The computational parameters are as follows: σ_{move}
557 = 30 years, σ_{change} and σ_{birth} = 4° for declination and 2° for inclination, K_{max} = 150, a chain
558 length of 200 million samples, priors of -25° and 30° for the minimum and maximum
559 declination, respectively, 50° and 75° for the minimum and maximum inclination,
560 respectively, and one datum age perturbed per age-resampling step.

561

562 **Table S1.** The archeomagnetic directions used for the dating methods described in this study.
563 Location of the sites: Anet (λ = 48.84956°N, ϕ = 1.42370°E); Genas (λ = 45.73229°N, ϕ =
564 4.99597°E); Plessis-Gassot (λ = 49.04653°N, ϕ = 2.41764°E).

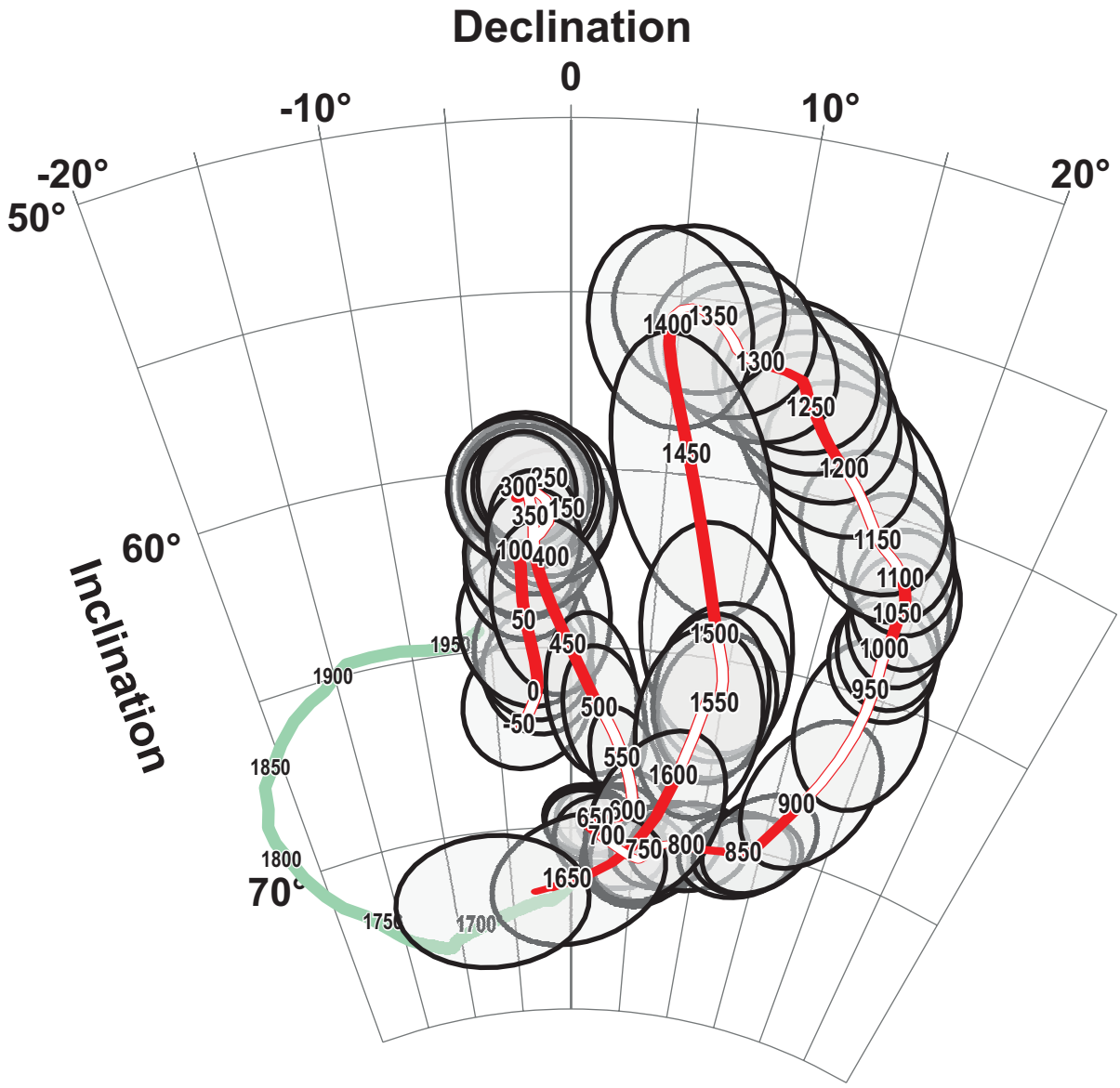
Declination
0
-10°
10°
-20°
20°
50°
60°
70°
Inclination
1400
1350
1300
1250
1200
1150
1100
1050
1000
950
900
850
800
750
700
650
600
550
500
450
400
350
300
250
200
150
100
50
0
-50
1450
1500
1550
1600
1650
1700
1750
1800
1850
1900
1950

Figure 1

a) Anet, upper floor

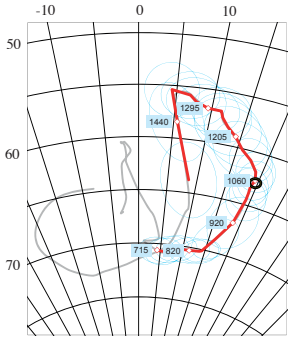

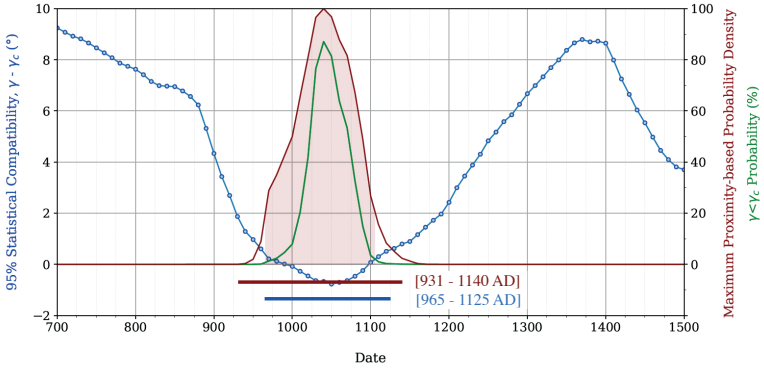

Synthetic dating

b)

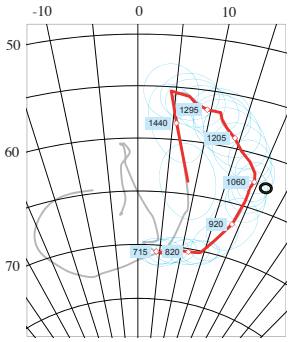

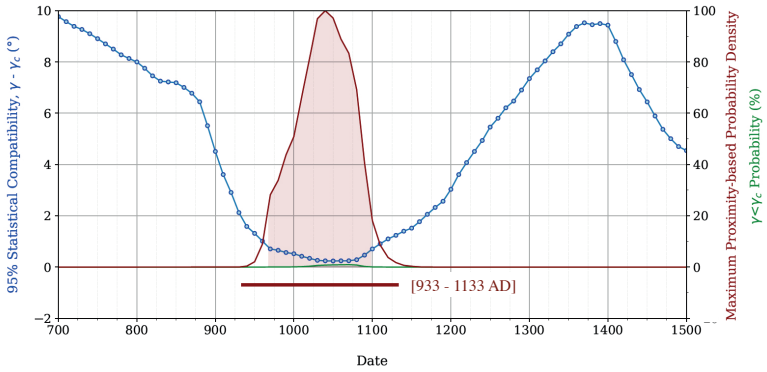

c)

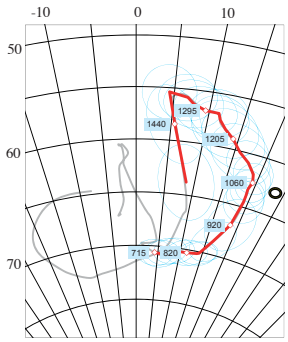

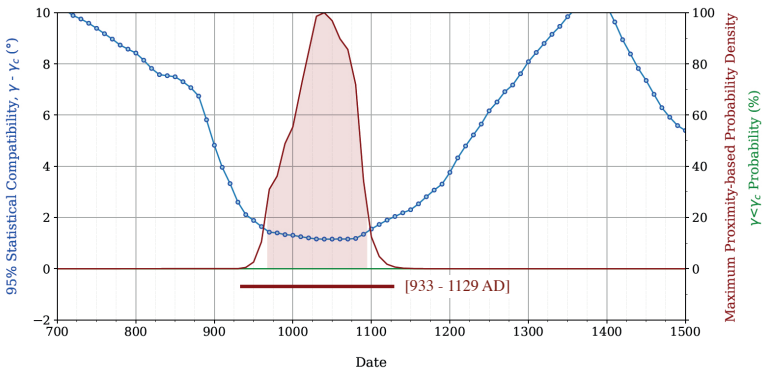

Figure 2

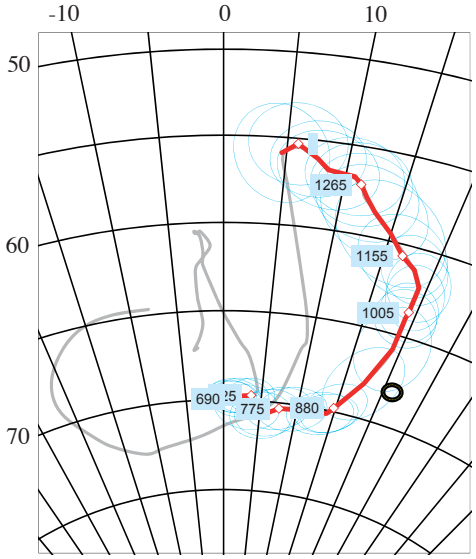
-10
0
10
50
60
70
1265
1155
1005
690
775
880

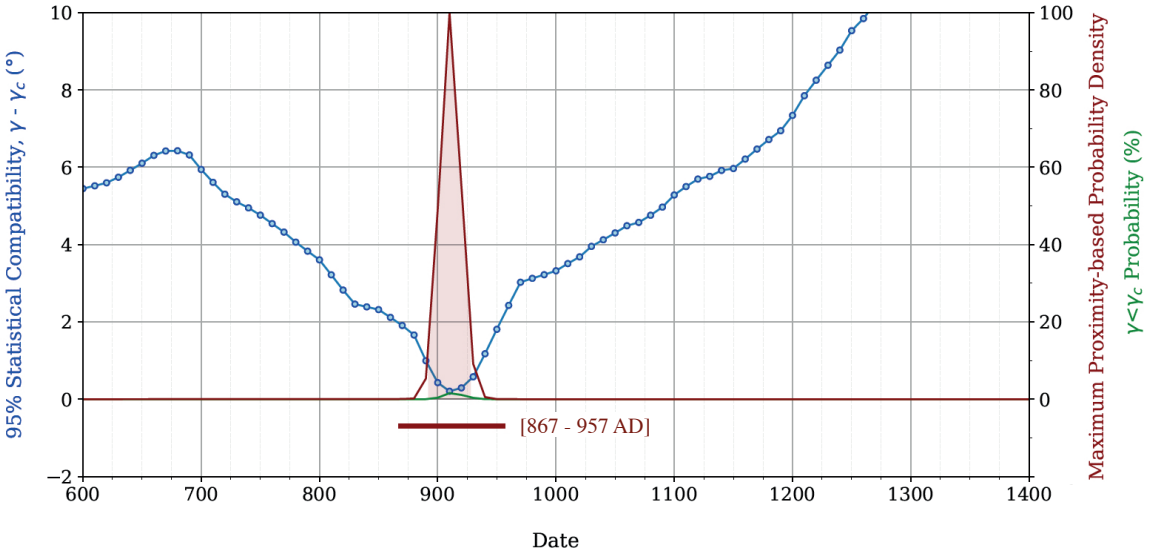
95% Statistical Compatibility, γ - γc (°)
Maximum Proximity-based Probability Density
γ<γc Probability (%)
Date
[867 - 957 AD]
10
8
6
4
2
0
−2
100
80
60
40
20
0
600
700
800
900
1000
1100
1200
1300
1400

Figure 3

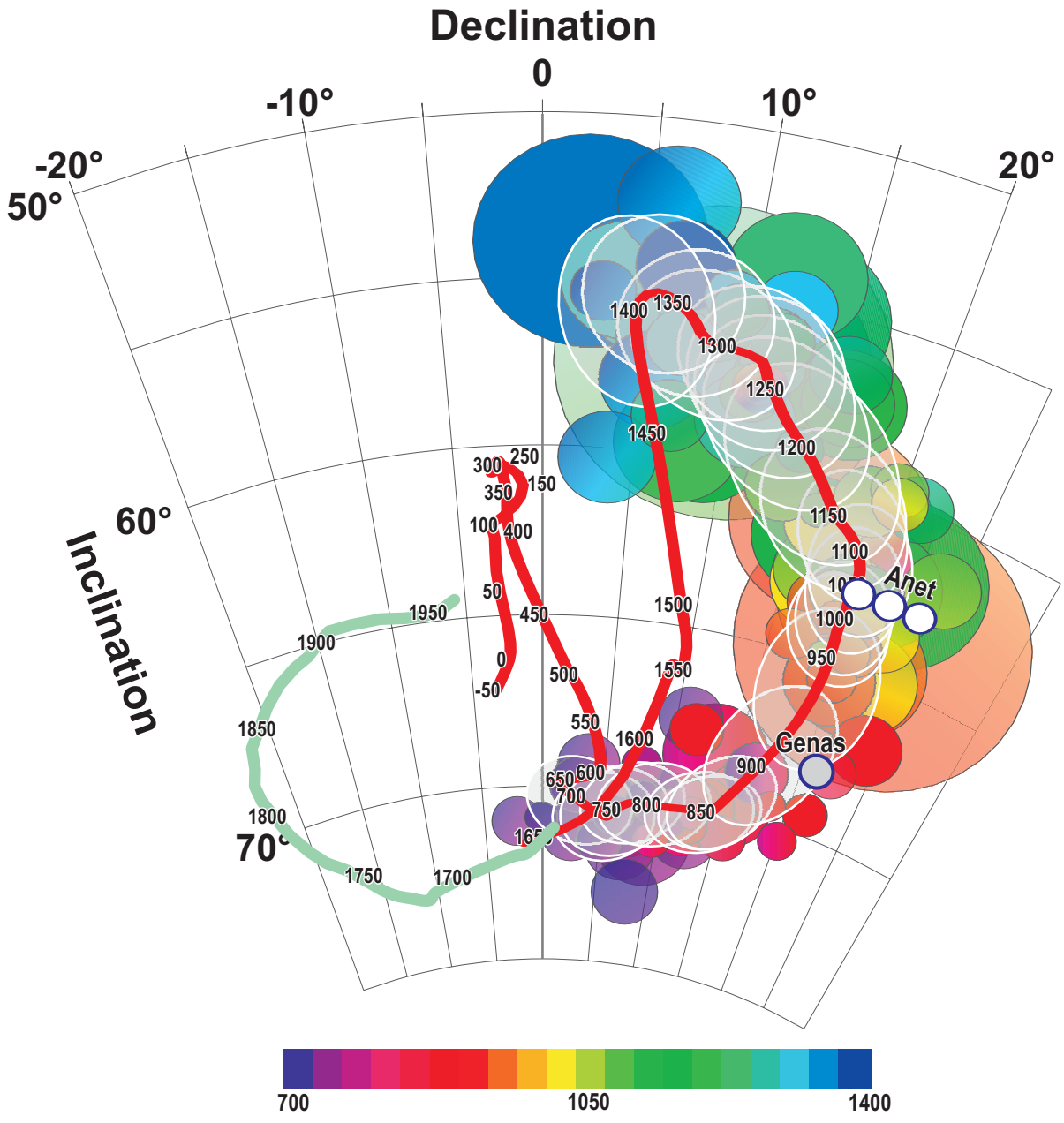
Declination
0
-10°
10°
-20°
20°
50°
60°
70°
Inclination
Anet
Genas
1400
1350
1300
1250
1200
1150
1100
1000
950
900
850
800
750
700
650
600
550
500
450
400
350
300
250
150
100
50
0
-50
1450
1500
1550
1600
1700
1750
1800
1850
1900
1950
700
1050
1400

Figure 4

a) Plessis-Gassot

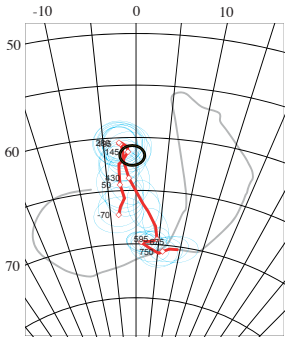

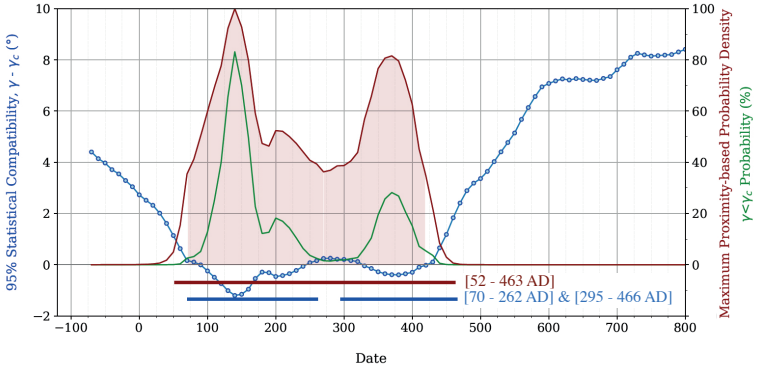

Synthetic dating

b)

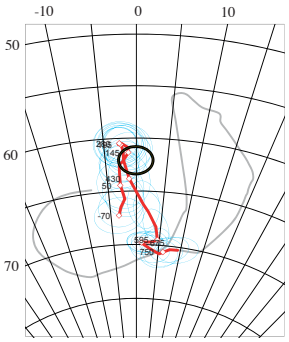

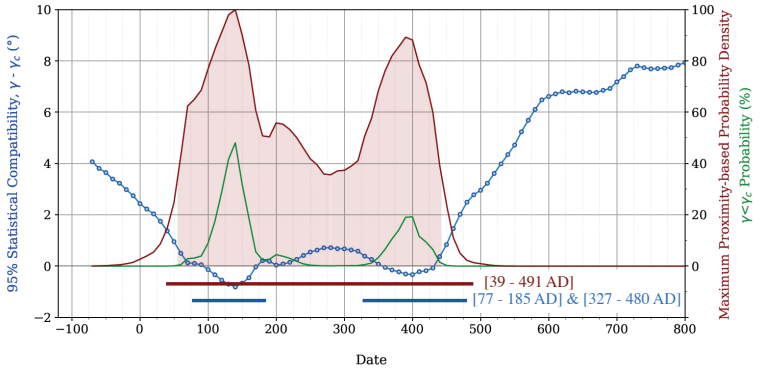

c)

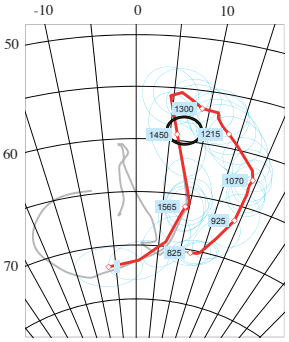

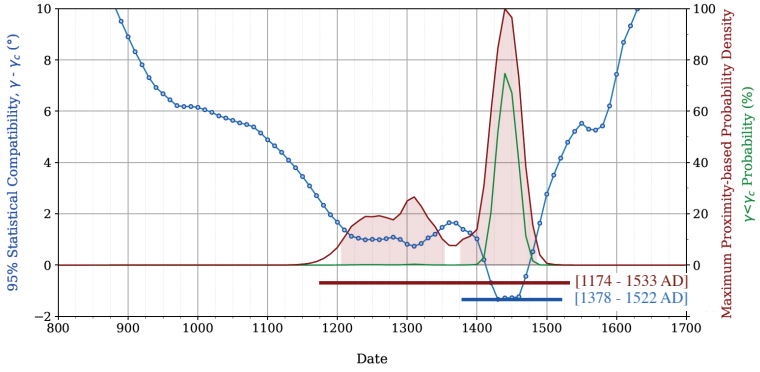

Figure 5

a)

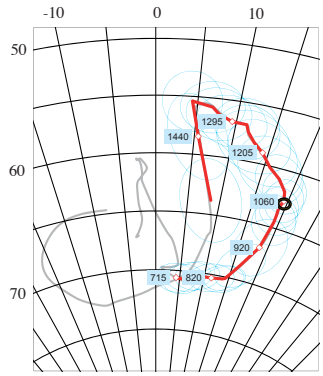
-10
0
10
50
60
70
1295
1440
1205
1060
920
715
820

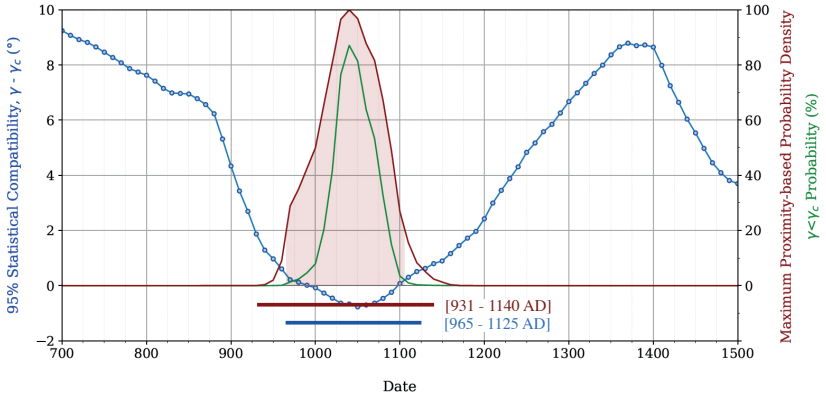
95% Statistical Compatibility, γ - γc (°)
Maximum Proximity-based Probability Density
γ<γc Probability (%)
[931 - 1140 AD]
[965 - 1125 AD]
Date

b)

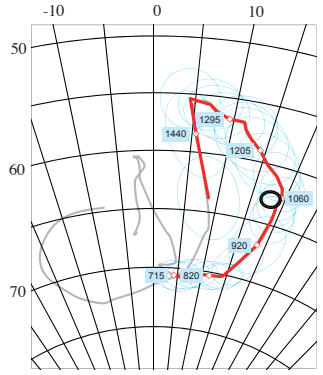
-10
0
10
50
60
70
1295
1440
1205
1060
920
715
820

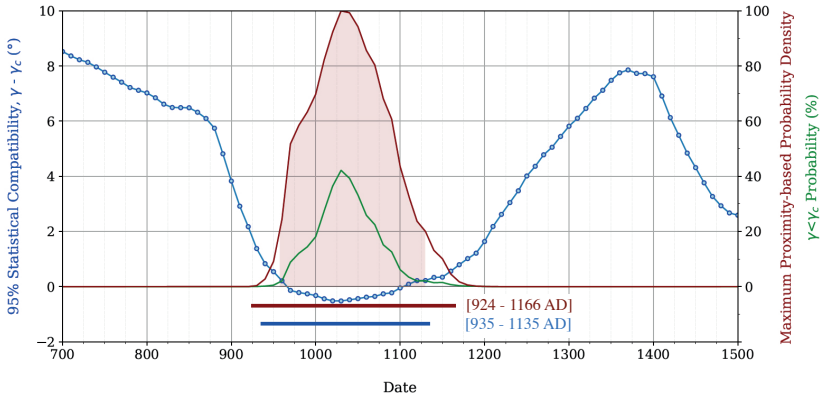
95% Statistical Compatibility, γ - γc (°)
Maximum Proximity-based Probability Density
γ<γc Probability (%)
[924 - 1166 AD]
[935 - 1135 AD]
Date

c)

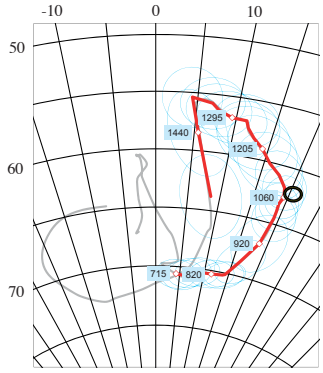
-10
0
10
50
60
70
1295
1440
1205
1060
920
715
820

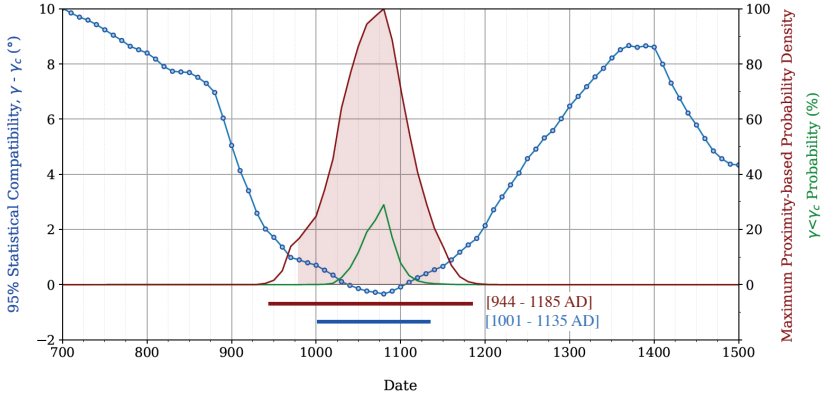
95% Statistical Compatibility, γ - γc (°)
Maximum Proximity-based Probability Density
γ<γc Probability (%)
[944 - 1185 AD]
[1001 - 1135 AD]
Date

Figure 6

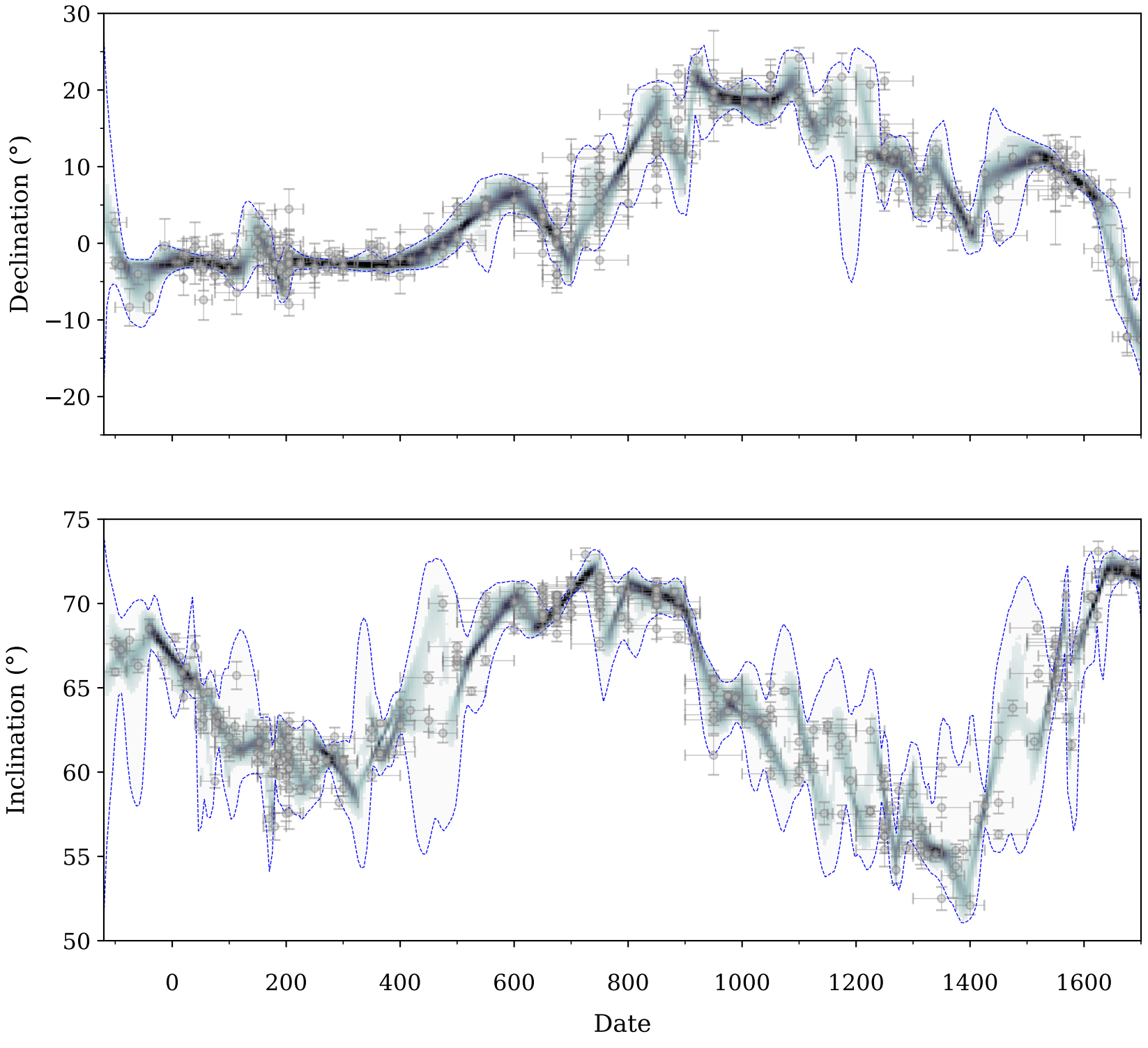
Declination (°)
30
20
10
0
−10
−20
Inclination (°)
75
70
65
60
55
50
0
200
400
600
800
1000
1200
1400
1600
Date

Figur
e A

Site	Declination site (°)	Inclination site (°)	Declination Paris (°)	Inclination Paris (°)	N samples	K	α95
Anet, upper floor (Fig. 2a, 6a)	19.6	62.6	19.6	62.8	23	4732	0.4
intermed. floor (Fig. 6b)	17.7	62.8	17.9	62.9	14	3138	0.7
lower floor (Fig. 6c)	20.3	61.9	20.5	62.1	22	2657	0.6
Genas (Fig. 3)	19.7	66.4	21.1	68.1	19	5820	0.4
Plessis-Gassot (Fig. 5a)	-0.6	61.9	-0.6	61.7	12	1869	0.9
Synthetic Roman (Fig. 5b)	-	-	-0.1	62.1	13	892	1.3
Synthetic Medieval (Fig. 5c)	-	-	7.0	59.0	13	892	1.3

Table S1